IEEE Access
Multidisciplinary | Rapid Review | Open Access Journal

Received January 6, 2020, accepted January 13, 2020, date of publication January 15, 2020, date of current version January 28, 2020.

Digital Object Identifier 10.1109/ACCESS.2020.2966876

Adaptive Fault Isolation and System Reconfiguration Method for GNSS/INS Integration

CHUANG ZHANG, XIUBIN ZHAO, CHUNLEI PANG, TENGYAO LI, AND LIANG ZHANG
Information and Navigation College, Air Force Engineering University, Xi'an 710077, China

Corresponding author: Chunlei Pang (chunleipcl@163.com)

This work was supported in part by the National Natural Science Foundation of China under Grant 61601506 and Grant 41904014.

ABSTRACT Appropriate fault isolation and system reconfiguration scheme is of great significance to ensure the reliability and precision of the tightly coupled global navigation satellite system/inertial navigation system (GNSS/INS). Currently, the commonly used methods include fault isolation method and fault adaptation method. However, the performance of them is not compared and analyzed fully in the existing literatures. In this paper, the principle of them is analyzed and the performance of them under different conditions is compared in theory firstly. On this basis, to improve the effectiveness and adaptability of fault detection and isolation, an adaptive fault isolation and system reconfiguration method is proposed. The radial basis function neural network (RBFNN) is used to predict the pseudo-GNSS measurement for the measurement reconfiguration. Besides, taking the variety of observation conditions into consideration, an adaptive adjustment criterion is introduced to realize the switch of fault isolation and measurement reconfiguration. The performance of the proposed method is verified and compared with the traditional methods by using the field test data. The results show that the fault isolation method can obtain higher filtering precision than the fault adaptation method in theory, compared with these two methods, the proposed method has better adaptability to the complex environment, and can improve the reliability and precision of the navigation system effectively.

INDEX TERMS Tightly coupled GNSS/INS integration, fault isolation and system reconfiguration, fault adaptation, radial basis function neural network, measurement reconfiguration.

I. INTRODUCTION

The tightly coupled integration of global navigation satellite system (GNSS) and inertial navigation system (INS) can achieve a superior performance to the single system as a result of the good complementary characteristics [1]. However, the integration can't always offer reliable and accurate navigation information due to the faulty observations of navigation sensors [2]. If the faulty measurements are not detected and isolated in time, the accuracy of the integrated navigation will be directly affected. Therefore, the real time fault detection and isolation is of great importance to ensure the reliability and precision of the integrated navigation system [3].

In the field of integrated navigation, the commonly used fault detection methods can be divided into two categories: one is the snapshot method, such as the chi-square detection method [4]-[6], Multiple Solution Separation (MSS) [7], [8]. This kind of method can detect the abrupt faults quickly and accurately, but the performance for gradual fault is not very good as a result of the serious time delay. The other one is the sequential method, including the Autonomous Integrity Monitoring by Extrapolation (AIME) method [9], [10], Optimal Fault Detection (OFD) [11]. In these methods, the measurements used to calculate the test statistic are not limited to a single epoch. Therefore, compared to the snapshot method, these methods have better detection performance for gradual fault. To further improve the sensibility for gradual fault, a lot of modified methods have been proposed. A new rate detector algorithm based on AIME was developed in [12] and the test results show that it has better detection performance than AIME and MSS for gradual fault. A fast gradual fault detection method based on improved residual

The associate editor coordinating the review of this manuscript and approving it for publication was Mu Zhou.

chi-square detection method was proposed for underwater integrated navigation systems [13]. Besides, fault detection based on artificial intelligence has attracted more attention and been widely studied. Adaptive Neuron Fuzzy Inference System (ANFIS)-based approach was presented for detecting the navigation sensor faults in UAVs [14]. Reference [15] proposed a novel fault detection method based on Gaussian Process Regression (GPR) to improve the detection performance for gradual fault. Least Squares Support Vector Machine (LS-SVM) have been used for detecting fault in INS/GPS integration [11].

However, the above researches mainly aimed at how to detect the fault accurately and fast, the fault isolation and system reconfiguration, which is another key issue of the fault detection and tolerance, was seldom considered. In multi-sensor integration, usually the faulty sub-filter is isolated and the measurement update process is accomplished by fusing the results of the other normal sub-filters [13]. In GNSS/INS integration, isolating the faulty subsystem will force the integrated system into the pure INS model, which will result in the decrease of the filtering precision [16]. Currently, the commonly used fault isolation method is identifying and isolating the faulty measurement by conducting the local test [17], [18]. After the isolation of the faulty measurements, the other normal measurements will be used for the measurement update process of the filter. This method reserves more useful measurements, therefore, compared with the method isolating the faulty sub-system, it has higher precision. However, the performance of this method is affected by the satellite configuration and fault duration time [19], and the difference of the location of faulty measurements will also lead to different filtering precision and fault detection results. Another fault isolation and system reconfiguration method is the detection, identification and adaptation (DIA) method [20], [21]. This method eliminates the presence of biases in the filtered state of the navigation system by estimating the model error. Nevertheless, the performance of this method is seldom analyzed and verified in the existing literatures, and the relation between this method and the fault isolation method is rarely compared and analyzed in theory.

Apart from the above two methods, the robust estimation is another way to improve the precision and reliability of the integrated navigation under fault conditions. The core idea of robust estimation is adaptively adjusting the weight of the measurement by equivalent weight function [22]-[24]. The typical equivalent weight function includes the three-segment function and two-segment function [25]. The two-segment function can maintain more measurements by reducing the weight of faulty measurement. Compared with the former, the three-segment function can eliminate the outlier from the measurements when the fault error is large enough by setting the adaptive weight factor of faulty measurement as zero. However, the performance of the two robust estimation methods depend on the selection of weight matrix a lot [26].

In practical application, the observation conditions and fault models are variant, each method may not be suitable for all the scenarios. In this paper, to have an overall understanding of the performance of the existing methods, we mainly analyze the principle of the fault isolation method and fault adaptation method, and then compare the performance of them under different conditions in theory. In order to overcome the drawbacks of these two methods, an adaptive fault isolation and system reconfiguration method is proposed. A new predictor based on radial basis function neural network (RBFNN) that can reduce the dependence on the motion state of vehicle is used to predict the pseudo-GNSS measurement for the measurement reconfiguration. Besides, an adaptive adjustment criterion is introduced to realize the switch of fault isolation and measurement reconfiguration, which improves the adaptability of fault detection and isolation method to the complex environment. Field test data are used to evaluate the proposed method, and the performance is compared with the conventional methods.

The paper is organized as follows. Section II introduces the fault detection and identification method for GNSS/INS integration. Section III describes the principle of fault isolation method and fault adaptation method, and then analyzes and compares the performance of them in theory. Section IV proposes the adaptive fault isolation and system reconfiguration scheme. Section V presents the experimental results. Section VI discusses the conclusions.

II. FAULT DETECTION AND IDENTIFICATION FOR GNSS/INS INTEGRATION

A. GNSS/INS INTEGRATION MODEL

For the tightly coupled GNSS/INS integration, the system state model consists of the error state equations of both INS and GNSS, and is usually expressed as

$$\dot{\mathbf{X}} = \mathbf{F}\mathbf{X} + \mathbf{G}\mathbf{W} \tag{1}$$

where $\mathbf{X} = [\boldsymbol{\Phi}, \delta\mathbf{V}, \delta\mathbf{P}, \boldsymbol{\varepsilon}, \boldsymbol{\nabla}, \delta t_u, \delta t_{ru}]^T$ is the state vector, $\boldsymbol{\Phi} = [\phi_E, \phi_N, \phi_U]$ is the misalignment angle error vector, $\delta\mathbf{V} = [\delta v_E, \delta v_N, \delta v_U]$ is the velocity error vector. $\delta\mathbf{P} = [\delta L, \delta\lambda, \delta h]$ denotes the position error vector, $\boldsymbol{\varepsilon} = [\varepsilon_x, \varepsilon_y, \varepsilon_z]$ and $\boldsymbol{\nabla} = [\nabla_x, \nabla_y, \nabla_z]$ represent the gyro biases and accelerometer biases. δt_u,δt_{ru} are the range bias and range drift related to the receiver clock. $\mathbf{F}$ is the system dynamic matrix, $\mathbf{G}$ is the noise coefficient matrix, $\mathbf{W}$ is the system noise vector.

In the measurement model, the observation vector consists of the pseudorange and pseudorange rate differences between INS and GNSS. And the system measurement equation can be written as

$$\mathbf{Z} = \begin{bmatrix} \mathbf{Z}_\rho \\ \mathbf{Z}_{\dot\rho} \end{bmatrix} = \begin{bmatrix} \mathbf{H}_\rho \\ \mathbf{H}_{\dot\rho} \end{bmatrix} \mathbf{X} + \begin{bmatrix} \mathbf{V}_\rho \\ \mathbf{V}_{\dot\rho} \end{bmatrix} = \mathbf{H}\mathbf{X} + \mathbf{V} \tag{2}$$

where $\mathbf{Z}$, $\mathbf{H}$ and $\mathbf{V}$ denote the measurement vector, the measurement matrix and the measurement noise vector, respectively. $\mathbf{Z}_\rho$, $\mathbf{H}_\rho$ and $\mathbf{V}_\rho$represent the components for pseudorange, while $\mathbf{Z}_{\dot\rho}$, $\mathbf{H}_{\dot\rho}$ and $\mathbf{V}_{\dot\rho}$ represent the components for pseudorange rate. The detailed expressions of these parameters can be found in [27].

B. FAULT DETECTION AND IDENTIFICATION

The linear discrete time varying system model can be described as

$$\begin{cases} \mathbf{X}_k = \mathbf{\Phi}_{k,k-1}\mathbf{X}_{k-1} + \mathbf{\Gamma}_{k,k-1}\mathbf{W}_{k-1} \\ \mathbf{Z}_k = \mathbf{H}_k\mathbf{X}_k + \mathbf{V}_k \end{cases} \tag{3}$$

where $\mathbf{X}_k$ is the state vector, $\mathbf{\Phi}_{k,k-1}$ is the transition matrix, $\mathbf{\Gamma}_{k,k-1}$ is the coefficient matrix, $\mathbf{Z}_k$ represents the measurement vector, $\mathbf{H}_k$ is the measurement model matrix. $\mathbf{W}_k$ and $\mathbf{V}_k$ are the process noise and measurement noise, which are commonly assumed as zero-mean Gaussian white noise with covariance matrix $\mathbf{Q}_k$ and $\mathbf{R}_k$, respectively.

The residual vector in Kalman filter is

$$\mathbf{v}_k = \mathbf{Z}_k - \mathbf{H}_k\bar{\mathbf{X}}_{k,k-1} \tag{4}$$

where $\bar{\mathbf{X}}_{k,k-1} = \mathbf{\Phi}_{k,k-1}\hat{\mathbf{X}}_{k-1}$ is the predicted state with the covariance matrix $\mathbf{P}_{k,k-1}$.

The corresponding covariance of the residual vector can be expressed as

$$\mathbf{P}_{vk} = \mathbf{H}_k\mathbf{P}_{k,k-1}\mathbf{H}_k^T + \mathbf{R}_k \tag{5}$$

To detect and identify the faulty measurement, the fault detection function based on standardized residual is given as [28]

$$\lambda_k^i = \frac{\mathbf{c}_i^T\mathbf{P}_{vk}^{-1}\mathbf{v}_k}{\sqrt{\mathbf{c}_i^T\mathbf{P}_{vk}^{-1}\mathbf{c}_i}}, \quad i = 1, \cdots, n \tag{6}$$

where $\mathbf{c}_i$ is the unit vector with the ith element equal to one, and n is the dimension of the measurement vector. λ_k^i obeys the normal distribution. The fault detection criterion is

$$\begin{cases} \left|\lambda_k^i\right| > N_{\alpha/2}\,(0,1) & \text{fault occurs} \\ \left|\lambda_k^i\right| \le N_{\alpha/2}\,(0,1) & \text{no fault occurs} \end{cases} \tag{7}$$

where α is the false alarm rate, $N_{\alpha/2}\,(0,1)$ is the corresponding threshold. The faulty measurement can be detected and identified by testing each dimension of the residual vector.

III. TRADITIONAL FAULT ISOLATION AND SYSTEM RECONFIGURATION METHODS

A. SYSTEM RECONFIGURATION BASED ON THE ISOLATION OF FAULTY MEASUREMENT

The commonly used fault detection and isolation method conducts the measurement update of Kalman filter by using the remaining normal measurements after the fault isolation. For the convenience of analysis, assuming that fault occurs on the ith dimension of the measurement vector, after the isolation of the faulty measurement, the new measurement equation can be written as

$$\tilde{\mathbf{Z}}_k = \begin{bmatrix} \mathbf{Z}_k^1 \\ \cdots \\ \mathbf{Z}_k^{i-1} \\ \mathbf{Z}_k^{i+1} \\ \cdots \\ \mathbf{Z}_k^n \end{bmatrix} = \begin{bmatrix} \mathbf{H}_k^1 \\ \cdots \\ \mathbf{H}_k^{i-1} \\ \mathbf{H}_k^{i+1} \\ \cdots \\ \mathbf{H}_k^n \end{bmatrix} \mathbf{X}_k + \begin{bmatrix} \mathbf{V}_k^1 \\ \cdots \\ \mathbf{V}_k^{i-1} \\ \mathbf{V}_k^{i+1} \\ \cdots \\ \mathbf{V}_k^n \end{bmatrix} = \tilde{\mathbf{H}}_k\mathbf{X}_k + \tilde{\mathbf{V}}_k \tag{8}$$

where $\mathbf{Z}_k^i$, $\mathbf{H}_k^i$ and $\mathbf{V}_k^i$ are the $i$throw element of $\mathbf{Z}_k$, $\mathbf{H}_k$and $\mathbf{V}_k$, respectively. Then, the new state estimation $\tilde{\mathbf{X}}_k$ and its covariance matrix $\tilde{\mathbf{P}}_{ki}$ can be written as

$$\begin{aligned} \tilde{\mathbf{X}}_k &= \tilde{\mathbf{P}}_{ki}\left(\mathbf{P}_{k,k-1}^{-1}\bar{\mathbf{X}}_{k,k-1} + \tilde{\mathbf{H}}_k^T\tilde{\mathbf{R}}_k^{-1}\tilde{\mathbf{Z}}_k\right) \\ \tilde{\mathbf{P}}_{ki} &= \left(\mathbf{P}_{k,k-1}^{-1} + \tilde{\mathbf{H}}_k^T\tilde{\mathbf{R}}_k^{-1}\tilde{\mathbf{H}}_k\right)^{-1} \end{aligned} \tag{9}$$

where $\tilde{\mathbf{R}}_k$ is the noise covariance matrix of the remaining measurements.

B. FAULT ADAPTATION BASED ON OPTIMAL MODEL ERROR ESTIMATION

The fault adaptation method is based on the optimal model error estimation to eliminate the presence of biases on the state estimation. Similarly, assuming that fault error occurs on the ith measurement, then the measurement model can be written as

$$\mathbf{Z}_k = \mathbf{H}_k\mathbf{X}_k + \mathbf{V}_k + \mathbf{e}_i\nabla \tag{10}$$

where $\nabla$is the model error on the ith observation, and$\mathbf{e}_i$ is the unit vector with the ith element equal to one.

The optimal estimation of model error can be obtained as

$$\hat{\nabla} = \left(\mathbf{e}_i^T\mathbf{P}_{vk}^{-1}\mathbf{e}_i\right)^{-1}\mathbf{e}_i^T\mathbf{P}_{vk}^{-1}\mathbf{v}_k \tag{11}$$

The corresponding covariance of $\hat{\nabla}$ can be expressed as

$$\begin{aligned} \mathbf{P}_{\hat{\nabla}} &= \left(\mathbf{e}_i^T\mathbf{P}_{vk}^{-1}\mathbf{e}_i\right)^{-1} \\ &= \left(P_{vk}^{-1}{}_{ii}\right)^{-1} \end{aligned} \tag{12}$$

where $P_{vk}^{-1}{}_{ii}$ is the ith diagonal element of covariance matrix $\mathbf{P}_{vk}^{-1}$. Then, the new measurement model after adaptation can be expressed as $\widehat{\mathbf{Z}}_k = \mathbf{Z}_k - \mathbf{e}_i\hat{\nabla} = \mathbf{H}_k\mathbf{X}_k + \boldsymbol{\xi}_k$, where $\boldsymbol{\xi}_k$ is the new measurement noise and its covariance matrix $\widehat{\mathbf{R}}_k$is approximately to $\mathbf{R}_k + \mathbf{e}_i\mathbf{P}_{\hat{\nabla}}\mathbf{e}_i^T$, which ignores the correlation between $\mathbf{V}_k$ and $\hat{\nabla}$. Then, the state estimation at time k and its covariance matrix can be approximately expressed as

$$\begin{aligned} \widehat{\mathbf{X}}_k &= \widehat{\mathbf{P}}_k\left(\mathbf{P}_{k,k-1}^{-1}\bar{\mathbf{X}}_{k,k-1} + \mathbf{H}_k^T\widehat{\mathbf{R}}_k^{-1}\widehat{\mathbf{Z}}_k\right) \\ \widehat{\mathbf{P}}_k^{-1} &= \mathbf{P}_{k,k-1}^{-1} + \mathbf{H}_k^T\widehat{\mathbf{R}}_k^{-1}\mathbf{H}_k \end{aligned} \tag{13}$$

C. PERFORMANCE COMPARISON OF THE TWO METHODS

In [19], the influence of satellite configuration and fault duration time on the performance of fault isolation method has been analyzed and verified. Therefore, in this paper, the relation between fault isolation and fault adaptation is mainly analyzed and compared.

For the fault adaptation method, the optimal estimation of the single model error can be obtained as

$$\begin{aligned} \hat{\nabla} &= \left(\mathbf{e}_i^T\mathbf{P}_{vk}^{-1}\mathbf{e}_i\right)^{-1}\mathbf{e}_i^T\mathbf{P}_{vk}^{-1}\mathbf{v}_k \\ &= \left(\mathbf{P}_{vk\ ii}^{-1}\right)^{-1}\mathbf{P}_{vk\ i}^{-1}\mathbf{v}_k \\ &\approx \mathbf{v}_k^i \end{aligned} \tag{14}$$

where $\mathbf{P}_{vk\ i}^{-1}$ and v_k^i are the ith row of $\mathbf{P}_{vk}^{-1}$ and $\mathbf{v}_k$, respectively. Then, the new residual vector $\tilde{\mathbf{v}}_k$ and $\widehat{\mathbf{v}}_k$ of the fault isolation method and fault adaptation method can be expressed as

$$\begin{aligned}\tilde{\mathbf{v}}_k &= \left[\begin{array}{cccccc} v_k^1 & \cdots & v_k^{i-1} & v_k^{i+1} & \cdots & v_k^n \end{array}\right]^T \\ \widehat{\mathbf{v}}_k &= \left[\begin{array}{cccccc} v_k^1 & \cdots & v_k^{i-1} & \Delta v_k^i & v_k^{i+1} & \cdots & v_k^n \end{array}\right]^T \end{aligned} \tag{15}$$

where Δv_k^i is the ith row element of the new residual vector $\widehat{\mathbf{v}}_k$ and it's the difference between $\hat{\nabla}$ and v_k^i. According to (14), $\Delta v_k^i \approx 0$can be established. From the expressions of $\tilde{\mathbf{v}}_k$ and $\widehat{\mathbf{v}}_k$, it can be seen that there is nearly no new measurement information added in the measurement update of the fault adaptation method compared with the fault isolation method.

Based on the theory of Kalman filter, the gain matrix $\tilde{\mathbf{K}}_k$ and $\widehat{\mathbf{K}}_k$ of the isolation method and the adaptation method can be given as

$$\begin{aligned}\tilde{\mathbf{K}}_k &= \tilde{\mathbf{P}}_{ki}\tilde{\mathbf{H}}_k^T\tilde{\mathbf{R}}_k^{-1} \\ \widehat{\mathbf{K}}_k &= \widehat{\mathbf{P}}_k\mathbf{H}_k^T\widehat{\mathbf{R}}_k^{-1}\end{aligned} \tag{16}$$

where

$$\begin{aligned}\tilde{\mathbf{R}}_k &= diag\left[\begin{array}{cccccc} R_k^1 & \cdots & R_k^{i-1} & R_k^{i+1} & \cdots & R_k^n \end{array}\right] \\ \widehat{\mathbf{R}}_k &= diag[\begin{array}{ccccccc} R_k^1 & \cdots & R_k^{i-1} & \left(R_k^i + \left(P_{vk\ ii}^{-1}\right)^{-1}\right) & R_k^{i+1} & \cdots & R_k^n \end{array}]\end{aligned}$$

where R_k^i is the$i$th diagonal element of covariance matrix $\mathbf{R}_k$. Then, the state estimation of the isolation method can be expressed as

$$\begin{aligned}\tilde{\mathbf{X}}_k &= \tilde{\mathbf{X}}_{k,k-1} + \tilde{\mathbf{K}}_k\tilde{\mathbf{v}}_k \\ &= \tilde{\mathbf{X}}_{k,k-1} + \tilde{\mathbf{P}}_{ki}\tilde{\Delta}_k\end{aligned} \tag{17}$$

where

$$\begin{aligned}\tilde{\Delta}_k = &\left[\begin{array}{cccccc} \left(\mathbf{H}_k^1\right)^T & \cdots & \left(\mathbf{H}_k^{i-1}\right)^T & \left(\mathbf{H}_k^{i+1}\right)^T & \cdots & \left(\mathbf{H}_k^n\right)^T \end{array}\right] \\ &\tilde{\mathbf{R}}_k^{-1}\left[\begin{array}{cccccc} \mathbf{v}_k^1 & \cdots & \mathbf{v}_k^{i-1} & \mathbf{v}_k^{i+1} & \cdots & \mathbf{v}_k^n \end{array}\right]^T\end{aligned}$$

In the same way, the corresponding state estimation of the adaptation method can be expressed as

$$\begin{aligned}\widehat{\mathbf{X}}_k &= \widehat{\mathbf{X}}_{k,k-1} + \widehat{\mathbf{K}}_k\widehat{\mathbf{v}}_k \\ &= \widehat{\mathbf{X}}_{k,k-1} + \widehat{\mathbf{P}}_k\widehat{\Delta}_k\end{aligned} \tag{18}$$

where

$$\begin{aligned}\widehat{\Delta}_k = &\left[\begin{array}{cccccc} \left(\mathbf{H}_k^1\right)^T & \cdots & \left(\mathbf{H}_k^{i-1}\right)^T & \left(\mathbf{H}_k^i\right)^T & \left(\mathbf{H}_k^{i+1}\right)^T & \cdots & \left(\mathbf{H}_k^n\right)^T \end{array}\right] \\ &\widehat{\mathbf{R}}_k^{-1}\left[\begin{array}{cccccc} \mathbf{v}_k^1 & \cdots & \mathbf{v}_k^{i-1} & \Delta\mathbf{v}_k^i & \mathbf{v}_k^{i+1} & \cdots & \mathbf{v}_k^n \end{array}\right]^T\end{aligned}$$

Combining the expressions of $\tilde{\Delta}$and $\widehat{\Delta}$, it can be obtained that $\tilde{\Delta} \approx \widehat{\Delta}$ is established. From (17) and (18), it can be seen that the difference between $\tilde{\mathbf{X}}_k$ and $\widehat{\mathbf{X}}_k$ is related to the one step prediction of state estimation $\tilde{\mathbf{X}}_{k,k-1}$, $\widehat{\mathbf{X}}_{k,k-1}$ and covariance matrix $\tilde{\mathbf{P}}_{ki}$, $\widehat{\mathbf{P}}_k$. According to the matrix theory, the relation between $\widehat{\mathbf{P}}_k$ and $\tilde{\mathbf{P}}_{ki}$ can be expressed as

$$\begin{aligned}\widehat{\mathbf{P}}_k &= \left[\tilde{\mathbf{H}}_k^T\tilde{\mathbf{R}}_k^{-1}\tilde{\mathbf{H}}_k + \mathbf{P}_{k,k-1}^{-1} + \left(\mathbf{H}_k^i\right)^T\left(R_k^i + \left(P_{vk\ ii}^{-1}\right)^{-1}\right)^{-1}\mathbf{H}_k^i\right]^{-1} \\ &= \left[\tilde{\mathbf{P}}_{ki}^{-1} + \left(\mathbf{H}_k^i\right)^T\left(R_k^i + \left(P_{vk\ ii}^{-1}\right)^{-1}\right)^{-1}\mathbf{H}_k^i\right]^{-1} \\ &= \tilde{\mathbf{P}}_{ki} - \tilde{\mathbf{P}}_{ki}\left(\mathbf{H}_k^i\right)^T\left[\left(R_k^i + \left(P_{vk\ ii}^{-1}\right)^{-1}\right)^{-1}\right. \\ &\qquad \left. + \mathbf{H}_k^i\tilde{\mathbf{P}}_{ki}\left(\mathbf{H}_k^i\right)^T\right]^{-1}\mathbf{H}_k^i\tilde{\mathbf{P}}_{ki} \\ &= \tilde{\mathbf{P}}_{ki} - \Delta\mathbf{P}_k\end{aligned} \tag{19}$$

From (19), it can be proved that the following equation is established

$$\widehat{P}_k^{jj} \le \tilde{P}_{ki}^{jj} \tag{20}$$

where $\widehat{P}_k^{jj}$ and $\tilde{P}_{ki}^{jj}$ are the jth diagonal element of covariance matrix $\widehat{\mathbf{P}}_k$ and $\tilde{\mathbf{P}}_{ki}$, respectively. Equation (20) indicates that the weight of residual in fault adaptation method will be smaller than that in fault isolation method. And the difference between them mainly depends on the difference of $\widehat{\mathbf{P}}_k$ and $\tilde{\mathbf{P}}_{ki}$.

Assuming that fault starts at time k. For $t > k$, the state estimation and its covariance matrix of the fault isolation method are expressed as $\tilde{\mathbf{X}}_t$and $\tilde{\mathbf{P}}_{ti}$, respectively, while the corresponding parameters of fault adaptation method are expressed as $\widehat{\mathbf{X}}_t$ and $\widehat{\mathbf{P}}_t$. As we all know that it takes time for the error to accumulate to a certain degree, so for $t > k$ the difference between $\widehat{\mathbf{P}}_t$ of the fault adaptation method and $\tilde{\mathbf{P}}_{ti}$ is relatively small in the early phase of fault period, and the state estimation of the two methods will be nearly the same. In other words, $\tilde{\mathbf{X}}_t \approx \widehat{\mathbf{X}}_t$ will be established for a period of time. As faults on different satellite's measurements will result in the various degrees of decline in filtering precision. When fault lasts for a period of time, the location of faulty measurement will have a great influence on the change of filtering precision, which will affect the difference between $\widehat{\mathbf{P}}_t$ and $\tilde{\mathbf{P}}_{ti}$.

When the measurement of faulty satellite has little effect on the filtering precision, isolating the faulty measurement will not result in obvious reduction of the filtering precision. For this situation, the difference between $\widehat{\mathbf{P}}_t$ and $\tilde{\mathbf{P}}_{ti}$ will maintain at a small level. Although the weight of residual in adaptation method is smaller than that in isolation method, the filtering precision of adaptation method will be just a little lower than that of isolation method. Therefore, for $t > k$, $\tilde{\mathbf{X}}_t \approx \widehat{\mathbf{X}}_t$will be established for a relatively long period of time. In other words, adopting one of the two methods to deal with the faulty measurement will lead to nearly the same filtering results.

However, when the measurement of faulty satellite has a great effect on the filtering precision, isolating the faulty

measurement may result in obvious decrease of the filtering precision. For this situation, with the fault duration time getting longer, the state estimation error will get larger, and the difference between $\widehat{\mathbf{P}}_t$ and $\tilde{\mathbf{P}}_{ti}$ will also get larger. After the fault lasts for a period of time, as the one step prediction of state vector contains a large error, the residual will have a great influence on the state estimation. Because $\widehat{P}_t^{jj}$ is obviously smaller than $\tilde{P}_{ti}^{jj}$, which will lead to that the weight of the residual in adaptation method is much smaller than that in isolation method. Hence, the precision of the state estimation $\widehat{\mathbf{X}}_t$ will be lower than that of $\tilde{\mathbf{X}}_t$. And with the fault duration time getting longer, the difference between $\tilde{\mathbf{X}}_t$ and $\widehat{\mathbf{X}}_t$ will get larger. In other words, the filtering error of the adaptation method will be apparently larger than that of the isolation method after the fault lasts for a long time.

If there is enough measurement redundancy, both the filtering errors of isolation method and adaptation method will increase gradually. However, if the number of visible satellites is small or the geometry of satellites is poor, both the two methods will result in fast decrease of the filtering precision and large state estimation errors.

IV. ADAPTIVE FAULT ISOLATION AND SYSTEM RECONFIGURATION

In terms of the above analysis, the results of the fault isolation method and fault adaptation method will be variant under different observation conditions. Especially when the number of visible satellites is small and the measurement of faulty satellite has a great effect on the filtering precision, both the two methods will have large estimation errors due to the lack of useful observations. Therefore, in order to improve the adaptability of fault detection and isolation method to the complex environment, a new fault isolation and system reconfiguration method is proposed.

A. MEASUREMENT RECONFIGURATION BASED ON RBFNN

For GNSS/INS integration, in order to compensate INS errors under the condition of lack of useful measurements, especially GNSS outages, many researchers introduced the error predicting and compensating method based on artificial intelligence (AI) [29]. These approaches include support vector machine [30], random forest regression [31], neural network [32], etc. Due to the good nonlinear function estimation property and learning ability, the neural network (NN) has drawn great attention and been widely used in the error compensation of integrated navigation during GNSS outages. A hybrid model of strong tracking Kalman filter and wavelet neural network was proposed to predict INS error during GPS outages [33]. A new multi-layer perceptron (MLP) network prediction model that set up the relation between INS information and the increments of GPS position was proposed, which improved the prediction accuracy [16]. A hybrid prediction method which combines the radial basis function neural network (RBFNN) and the time series analysis was

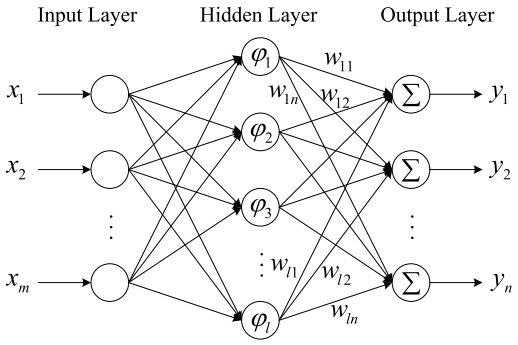

FIGURE 1. The structure of RBFNN.

proposed to predict the measurement update of Kalman filter during GPS outages in [34]. To improve the positioning precision of INS/GPS integration for long time GPS outages, a magnetometer-assisted positioning solution which uses the RBFNN predictor was introduced [35]. Although these approaches adopted different prediction model, compared with the pure INS mode, they can improve the positioning precision effectively.

However, the above researches mainly aims at the loosely coupled model of GNSS/INS integration. For the tightly coupled model, a fusion algorithm based on RBFNN for bridging GPS outages was proposed in [36], which used the past measurements to predict the measurements of current window, and then continued to predict the measurements in the next window. This method can improve the filtering precision during GPS outages, however, it's hard to choose a proper window size in practical application in real time. Besides, the performance of the method depends a lot on the motion state of the vehicle.

Compared with the other networks, the RBFNN is simpler to design and can learn faster with high accuracy. Therefore, in this paper, the RBFNN is used to obtain the pseudo-GNSS measurement when the faulty measurement is detected, which aims to provide a better fault isolation and system reconfiguration scheme. Usually, a RBFNN has a three-layer structure that consists of an input layer, a hidden layer and an output layer, which is shown in Fig. 1.

Where x_i $(i = 1, 2, \cdots, m)$ and y_i $(i = 1, 2, \cdots, n)$ are the inputs and outputs, while φ_i $(i = 1, 2, \cdots, l)$ is the base function, which is commonly selected as the Gaussian function, w_{ij} is the weight. The output y_i can be given as

$$y_i = \sum_{j=1}^{l} w_{ji}\phi_j(x) \tag{21}$$

As well known, the pseudorange and pseudorange rate measurements are time series information, which are affected by the motion state of the vehicle. Therefore, the measurement of INS is introduced to provide the motion constraint information, which helps to avoid the rapid divergence of the predicted measurements when the motion state changes. Here, $\delta\rho_G^i(k)$ and $\delta\rho_I^i(k)$ are defined as the pseudorange

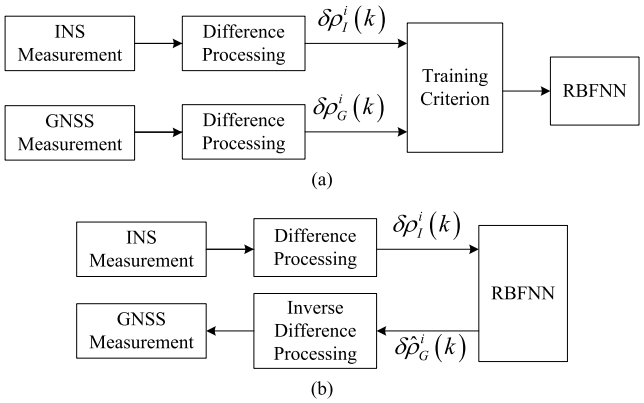

FIGURE 2. The update and prediction process of RBFNN. (a) The update process; (b) The prediction process.

increment of GNSS and INS for the *ith* satellite, which can be expressed as

$$\begin{aligned}\delta\rho_G^i(k) &= \rho_G^i(k+1) - \rho_G^i(k)\\ \delta\rho_I^i(k) &= \rho_I^i(k+1) - \rho_I^i(k)\end{aligned} \tag{22}$$

where ρ_G^i and ρ_I^i represent the pseudorange measurements of GNSS and INS for the *ith*satellite, respectively. In this paper, $\delta\rho_I^i(k)$ and $\delta\rho_G^i(k)$ are selected as the input and output of the network. Fig. 2 shows the update and prediction process of the RBFNN. Assuming that $\rho_G^i(j)$ contains a fault error and is detected at time j, then the pseudo-GNSS pseudorange measurement at time j can be obtained as

$$\hat{\rho}_G^i(j) = \rho_G^i(j-1) + \delta\hat{\rho}_G^i(j-1) \tag{23}$$

where $\delta\hat{\rho}_G^i(j-1)$ is the predicted pseudorange increment of GNSS. After a period of time, the pseudo-GNSS pseudorange at time t_k can be expressed as

$$\hat{\rho}_G^i(t_k) = \rho_G^i(j-1) + \sum_{t=j-1}^{t_k-1} \delta\hat{\rho}_G^i(t) \tag{24}$$

Then, the new pseudorange measurement of Kalman filter for the *ith* satellite at time t_k can be obtained as

$$\hat{Z}^i(t_k) = \rho_I^i(t_k) - \hat{\rho}_G^i(t_k) \tag{25}$$

The RBFNN for pseudorange rate is similar to that for pseudorange, the difference is that the input and output are replaced by the pseudorange rate increments of INS and GNSS.

B. ADAPTIVE ADJUSTMENT OF FAULT ISOLATION AND MEASUREMENT RECONFIGURATION

According to the analysis in section III, it can be seen that isolating the faulty measurement will lead to the decrease of the filtering precision, and the rate of decline will be variant for different observation conditions and location of faulty measurement. In order to evaluate the influence of a satellite's measurement on the precision of state estimation, several concepts are introduced. One is the precision of positioning (POP), which is chosen to evaluate the filter precision, and is expressed as

$$\text{POP}=\sqrt{\sum_{j=7}^{9}\hat{P}_k^{jj}} \tag{26}$$

where $\hat{P}_k^{jj}$ is the jth diagonal element of covariance matrix $\hat{\mathbf{P}}_k$. For the fault isolation method, $\hat{\mathbf{P}}_k$ is equal to$\tilde{\mathbf{P}}_k$, while for fault free condition, $\hat{\mathbf{P}}_k$ is equal to$\mathbf{P}_k$. Although POP just contains the covariance of positioning error, it can still reflect the state estimation precision to some degree. And the smaller the POP, the higher the precision of state estimation.

The other one is the relative differential precision of positioning (RDPOP), which is used to analyze the influence of one satellite's measurement on the filtering precision, and is expressed as

$$\text{RDPOP}=\frac{\sqrt{\sum_{j=7}^{9}\tilde{P}_{ki}^{jj}}-\sqrt{\sum_{j=7}^{9}P_k^{jj}}}{\sqrt{\sum_{j=7}^{9}P_k^{jj}}} \tag{27}$$

RDPOP reflects the decrease degree of positioning precision after isolating the satellite's measurement. The larger the RDPOP, the greater the decrease of filtering precision. When there are enough visible satellites, isolating the faulty measurement will hardly affect the filtering precision or just result in a very small decline of the filtering precision, which will not bring bad effect on the whole navigation and can be tolerant. For this situation, the good navigation performance can be obtained by adopting the traditional fault isolation method. Therefore, there is no need to use the predicted measurement to conduct the measurement reconfiguration.

However, when the geometry or number of visible satellites is poor, isolating the faulty measurement may lead to a fast decrease of the filtering precision, and the filtering error and RDPOP will get larger rapidly with the fault duration time getting longer, which will have a bad influence on the reliability of the navigation. For this situation, using the predicted measurement to conduct the measurement reconfiguration can restrain the divergence of filter and reduce the risk of missed detection and false alarm effectively. Therefore, to improve the adaptability of fault isolation and system reconfiguration method to the environment, an adaptive adjustment criterion is introduced and expressed as follows

$$\begin{cases}\text{POP} \le \xi & \text{fault isolation}\\ \text{POP} > \xi, \text{RDPOP} \le \eta & \text{fault isolation}\\ \text{POP} > \xi, \ \text{RDPOP} > \eta & \text{measurement reconfiguration}\end{cases} \tag{28}$$

where ξ and η are the thresholds of POP and RDPOP, and they can be chosen according to the requirement for the filtering precision.

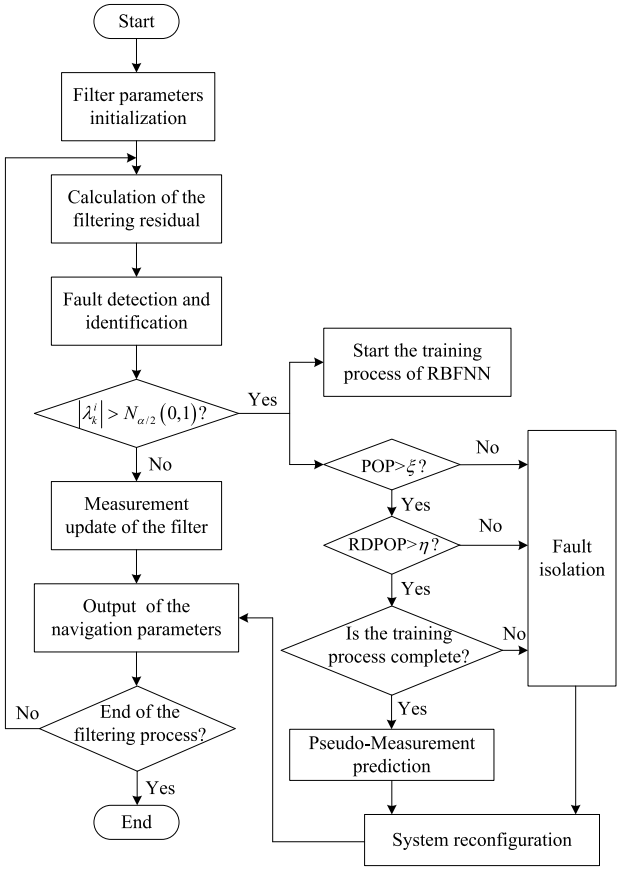

FIGURE 3. The flow chart of the adaptive fault isolation and system reconfiguration scheme.

TABLE 1. Inertial sensor technical specifications.

Parameters	Gyro	Accelerometer
Bias	20°/h	50mg
Bias stability	±1°/h	±0.75mg
Scale Factor	1500ppm	4000ppm

Based on the above analysis, the process of adaptive fault isolation and system reconfiguration scheme can be shown in Fig. 3. Here, it should be clearly noted that the training process of RBFNN is initiated after the fault is detected, which is aimed to reduce the computing burden. As the number of visible satellites is usually large, satellite observation failure is a rare event and the number of faulty satellites is usually small relatively, conducting the training process of RBFNN for all the satellites' measurements all the time will lead to great calculation burden on the navigation computer.

V. FIELD TEST RESULTS AND ANALYSIS

To verify the theoretical analysis and evaluate the performance of the proposed method, a low dynamic test was carried out in Xi'an, China. The SPAN-CPT tightly coupled navigation system was used to collect the raw IMU data and GNSS data. The output rate of inertial sensor and GNSS is

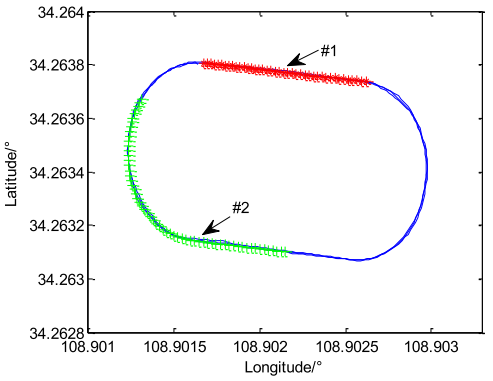

FIGURE 4. The vehicle trajectory.

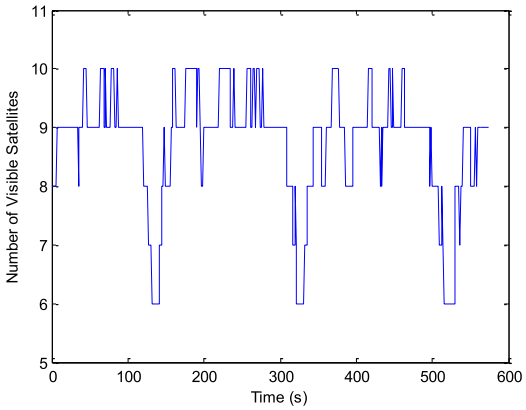

FIGURE 5. The number of GNSS visible satellites in the field test.

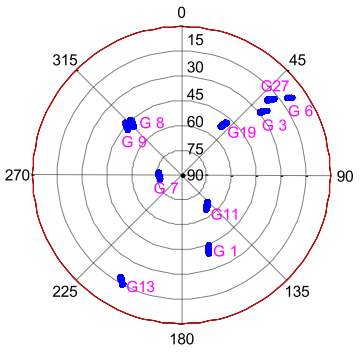

FIGURE 6. The sky plot view of the satellite geometry.

100Hz and 1Hz, respectively. The inertial sensor specifications of the SPAN-CPT are listed in Table 1. The experiment vehicle drove along the 400m sports track nearly three laps. The vehicle trajectory is shown in Fig. 4. The number of visible satellites in the field test is shown in Fig. 5, while the corresponding sky plot view is shown in Fig. 6.

A. THE PERFORMANCE ANALYSIS OF THE PROPOSED PREDICTION MODEL

In order to ensure that the proposed prediction method is able to provide the better performance in fault isolation and system reconfiguration, the performance of the proposed prediction model (M2) is verified and analyzed firstly, and the method in

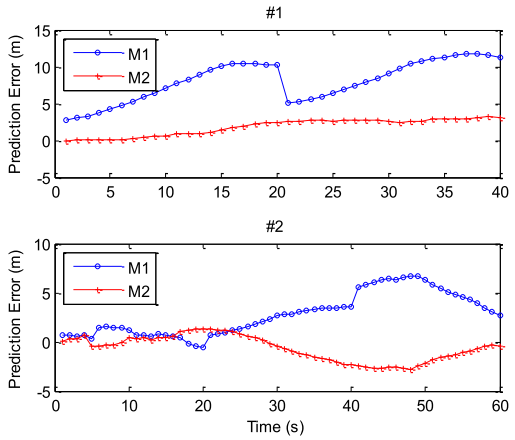

FIGURE 7. The prediction errors of the two methods.

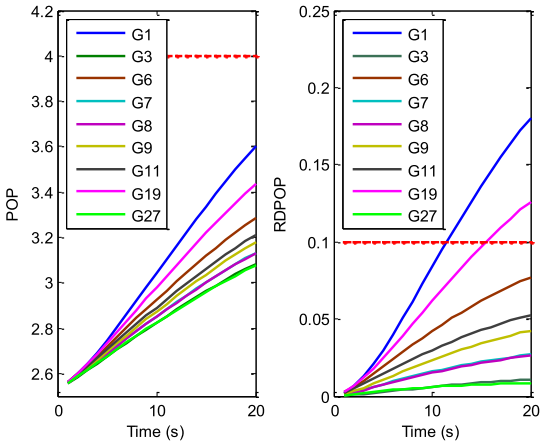

FIGURE 8. The POP and RDPOP of the nine visible satellites.

TABLE 2. Comparison of the prediction errors.

	MAD/m		RMSE/m	
	M1	M2	M1	M2
#1	8.06	1.83	8.51	2.14
#2	2.82	1.16	3.51	1.42

reference [36] (M1) is introduced for comparison. Set satellite G19 as an example, assuming that two segments of GNSS measurements for G19 contain fault errors, the first one is from 181s to 220s, while the second one is from 261s to 320s, the corresponding trajectories are marked by red and green lines in Fig. 4, respectively.

The prediction errors of the two methods during these two segments are shown in Fig. 7. It can be seen that the performance of M1 has large difference for the two segments of measurements, this is because that M1 depends a lot on the motion state of the vehicle. For the first segment, the state of the vehicle changes from circular motion to linear motion, so the prediction error is very large. For the second segment, when the prediction process starts, the state of the vehicle hardly change, so it can obtain high precision. As the state changes slowly, the prediction error begins to get larger, and for the last twenty seconds, the state of the vehicle changes from circular motion to linear motion, so the prediction error further increases. Compared with M1, the prediction accuracy of M2 is much higher, and the performance of M2 depends less on the motion state of the vehicle.

The mean absolute deviation (MAD) and root mean squared error (RMSE) of the prediction errors are calculated and shown in Table 2. It can be seen that the proposed prediction model has high precision and the predicted pseudo-measurement can be used to replace the faulty measurement within a period of time.

B. THE PERFORMANCE VERIFICATION AND ANALYSIS OF THE PROPOSED METHOD

In the tests, fault errors are attached to one satellite's measurements to simulate the fault scenario. The false alarm rate is set as 0.001, so the corresponding detection threshold is 3.29. To verify the performance of the proposed adaptive fault isolation and system reconfiguration method (AFISR), the results of the other two methods are introduced for comparison. The first one is the fault isolation method (FI), the other one is the fault adaptation method (FA). Besides, the results of fault free condition (FF) are also given for comparison. In this paper, the thresholds ξ and η are chosen as 4 and 0.1, respectively.

According to the analysis in Section III, it can be concluded that the performance of traditional fault isolation and system reconfiguration will be variant for the different observation conditions. Therefore, in the next parts, several tests under different measurement conditions and fault models will be conducted to verify the performance and superiority of the proposed method.

1) THE PERFORMANCE COMPARISON AND ANALYSIS FOR DIFFERENT NUMBERS OF VISIBLE SATELLITES

The number of visible satellite determines the observation redundancy to a large extent, which has a great influence on the filtering precision. Therefore, the performance of these methods under the condition of different numbers of visible satellites are tested firstly.

Test 1: Assuming that 100m abrupt fault error occurs on the measurement of one satellite from 281 to 300s, the visible satellites are G1, G3, G6, G7, G8, G9, G11, G19 and G27. During this period, there are enough observation redundancy. Fault on different satellite may result in variant navigation precision, so the POP and RDPOP of each satellite are calculated firstly, and the results are shown in Fig. 8.

It can be seen from Fig. 8 that the POP values of the nine satellites are less than 4 during the fault period, which means that the navigation can maintain high precision after isolating one satellite's measurements. Besides, it can be obtained that the POP and RDPOP of G1 are the largest among the nine visible satellites, while those of G27 are the smallest. In other words, isolating the measurements of G1 and G27 will result

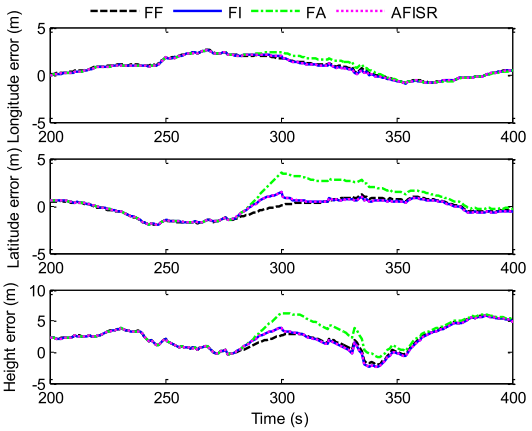

FIGURE 9. The position errors for fault on G1 under the condition of nine visible satellites.

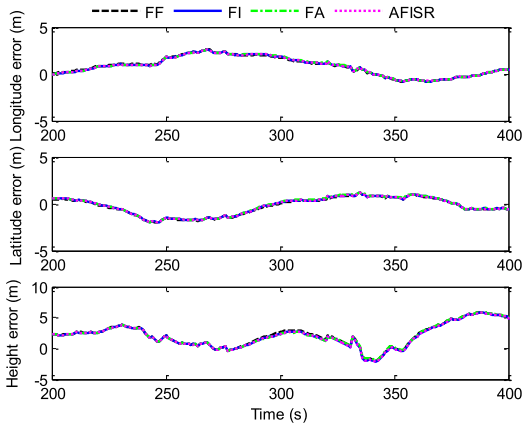

FIGURE 10. The position errors for fault on G27 under the condition of nine visible satellites.

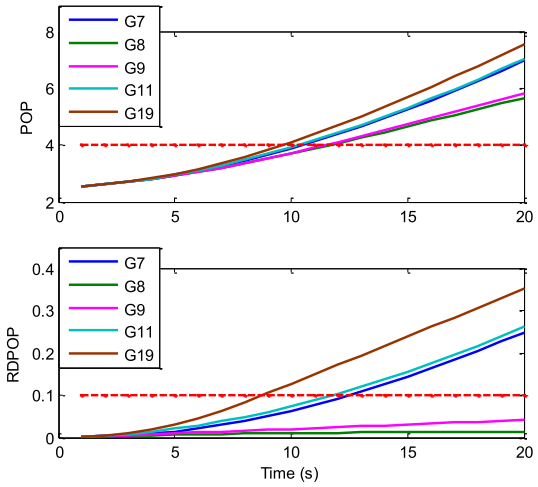

FIGURE 11. The POP and RDPOP of the five visible satellites.

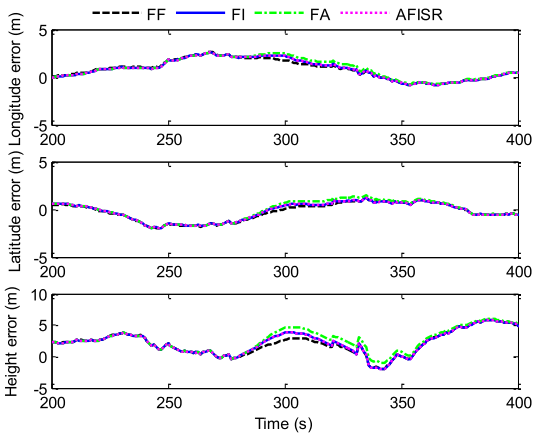

FIGURE 12. The position errors for 20s fault on G19 under the condition of nine visible satellites.

in the maximum and minimum decline of the filtering precision, respectively. Set satellite G1 and G27 as examples, the corresponding navigation results of the four methods are shown in Fig. 9 and Fig. 10.

It can be seen from Fig. 9 that the difference between the results of the four methods for fault on G1 is very obvious. Compared with the results of FF, the precision of FI is just a little lower, and as the POP is less than 4 during the whole fault period, the proposed AFISR changes into FI mode. The precision of FA is nearly the same as FI in the first few seconds of the fault period, however, with the fault time getting longer, the position errors begin to get larger, the precision of FA gradually gets lower than the other methods. It can be seen from Fig. 10 that the position errors of the four methods for fault on G27 are nearly the same. This is because that the measurement of G27 has little effect on the filtering precision and isolating the faulty measurement will not lead to obvious decline of the filtering precision.

Test 2: To simulate the case that the number of visible satellites is relatively small, several satellites' measurements are removed artificially from 281s to 300s, and only five of them are reserved, which are G7, G8, G9, G11 and G19. Similarly, assuming that 100m abrupt fault error occurs on the measurement of one satellite, the POP and RDPOP of each satellite are calculated and shown in Fig. 11.

It can be seen from Fig. 11 that as the fault duration time increases, all the POP values have a tendency to get larger and are greater than the threshold 4 at some point during the fault period. Among the five satellites, the POP and RDPOP of G19 are the largest, which means that isolating the measurement of G19 will result in the maximum decline of the filtering precision. Figs. 12 and 13 show the navigation results of the four methods for fault on G19 under the condition of nine and five satellites, respectively. It can be seen that compared with the results of FF, the position errors of the other three methods increase to some extent. When there are nine satellites, as the observation redundancy is relatively large, isolating the measurement of G19 just results in a small decline of the filtering precision. When there are only five satellites, the measurement of G19 has a great influence on the filtering precision. Both the geometry of satellites

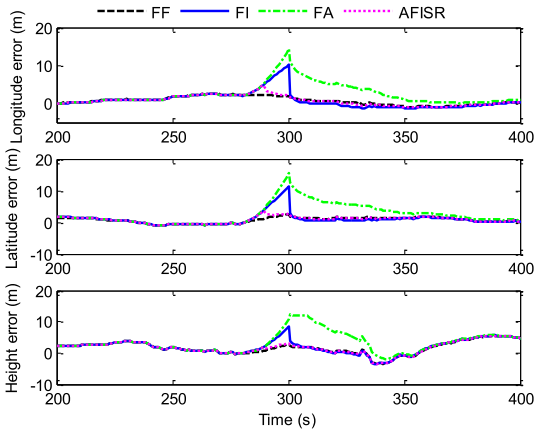

FIGURE 13. The position errors for 20s fault on G19 under the condition of five visible satellites.

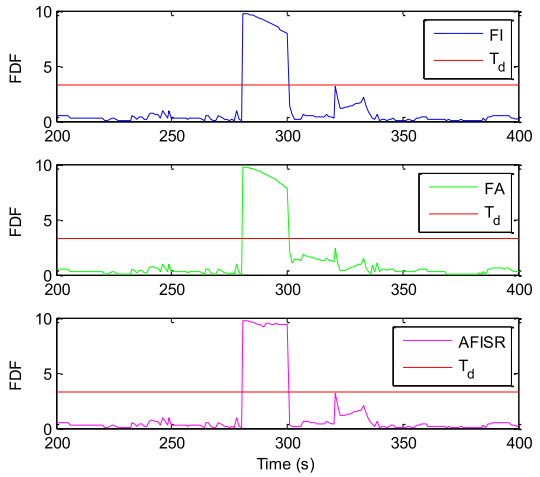

FIGURE 14. The FDFs of the three methods for 20s fault on G19.

and the observable degree of navigation parameters will get worse after isolating the measurement of G19. Therefore, the position errors of FI and FA get larger rapidly with time, and the precision is obviously much lower than that of FF when fault lasts for a period of time. Compared with FI and FA, the AFISR conducts the measurement update process by using the predicted pseudo-GNSS measurement from 290s, so the position errors of it gradually get smaller.

The corresponding fault detection function (FDF) of the three methods under the condition of five satellites are shown in Fig. 14. The red line represents the threshold of fault detection function, which is marked by T_d. It can be seen that the FDFs of FI and FA have an obvious downward trend due to the declined filtering precision, while the FDF of AFISR can maintain stable because of the high filtering precision.

In order to further verify the superiority of the proposed method, the situation with the longer fault duration time is investigated. Assuming that 100m abrupt fault error occurs on G19 from 261s to 320s, the navigation results of the four methods are shown in Fig. 15.

It can be seen that the position errors of FI and FA continue to increase with the fault duration time getting longer, and the

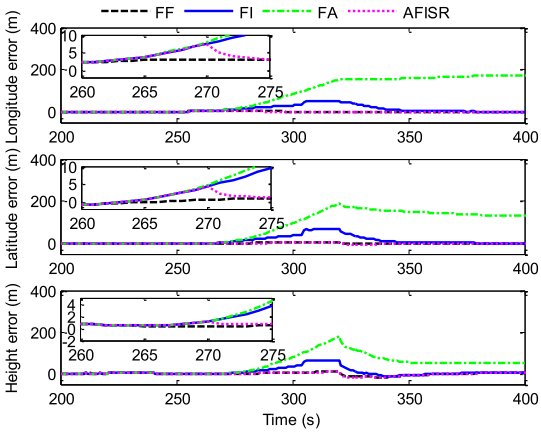

FIGURE 15. The position errors for 60s fault on G19 under the condition of five visible satellites.

TABLE 3. Comparison of the RMS of position errors during 60s fault period.

RMSE/m	Method			
	FF	FI	FA	AFISR
Longitude	2.24	32.2	77.6	2.58
Latitude	2.52	39.4	92.1	2.95
Height	5.23	37.3	82.6	5.47

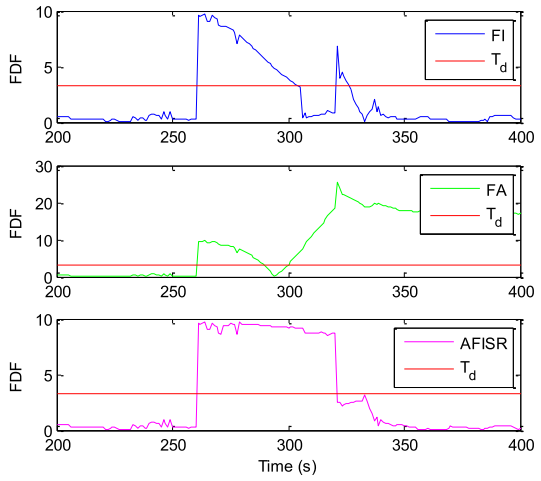

FIGURE 16. The FDFs of the three methods for 60s fault on G19.

maximum errors of FI for longitude, latitude and height are 57.8m, 67.5m and 66.9m, respectively, while those of FA are 155.2m, 190.6m and 181.5m, which are too large to provide reliable navigation. Compared with FI and FA, the position errors of AFISR reach to the maximum values at 270s, and then it switches to the new measurement update mode using the predicted pseudo-GNSS measurement, so the position errors gradually decrease. Table 3 shows the RMSE of these methods, it can be seen that compared with the conventional methods, the positioning accuracy is obviously improved by the proposed AFISR.

Fig. 16 shows the FDFs of the three methods, it can be seen that both the FDFs of the FI and FA have a rapid downward

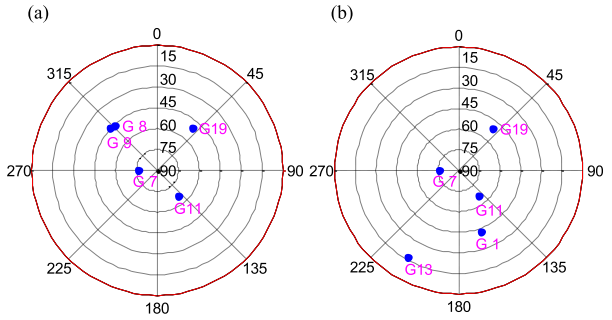

FIGURE 17. The sky plot views of two different geometries with five visible satellites. (a) geometry 1; (b) geometry 2.

trend, and the FDF value of FI at 305s is 3.19 that is smaller than the threshold, which results in the missed detection. After fault ends at 320s, the FDF has a few seconds of false alarm due to the large position errors. While the FDF of FA declines below the threshold at 290s and the missed detection happens during 290s∼300s. Similarly, after the end of fault at 320s, the false alarm happens and lasts for very long time due to the too large position errors. Compared with these two methods, the FDF of AFISR just has a gradual downward trend because of the high precision, which means that the AFISR can reduce the risk of missed detection and false alarm effectively.

2) THE PERFORMANCE COMPARISON AND ANALYSIS FOR DIFFERENT GEOMETRY OF VISIBLE SATELLITES

The above tests mainly investigate the influence of the number of visible satellites. In fact, when the number of satellites is constant, the geometry of satellites will also affect the navigation precision. For the same satellite in different geometries, its measurements will have different contribution to the filtering precision. And the effect is more obvious when the number of visible satellites is small. To further verify the performance of the proposed method, the number of visible satellites is set artificially as five, and two different geometries are chosen to conduct the tests. The first geometry consists of G7, G8, G9, G11 and G19, which lasts from 281s to 310s, while the second one consists of G1, G7, G11, G13 and G19, which lasts from 181s to 210s. The corresponding sky plot views are show in Fig. 17.

Set satellite G11 as an example, and 100m abrupt fault errors are attached to the measurements of G11 in these two periods. The POP and RDPOP of G11 in these two geometries are calculated and shown in Fig. 18. It can be seen that the POP and RDPOP in geometry 1 increase fast and exceed the thresholds in about 11 seconds, while the values in geometry 2 increase slowly, and the RDPOP is still smaller than the threshold when fault ends. This result indicates that the measurements of G11 have the greater influence on the filtering precision in geometry 1 than in geometry 2. In other words, isolating the measurements of G11 in geometry 1 may result in the worse filtering precision than in geometry 2.

The corresponding filtering results are shown in Fig. 19. And the RMS of position errors during the two fault periods

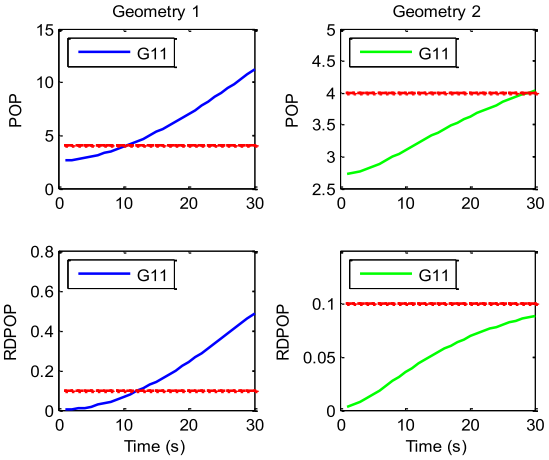

FIGURE 18. The POP and RDPOP of G11 for the two geometries.

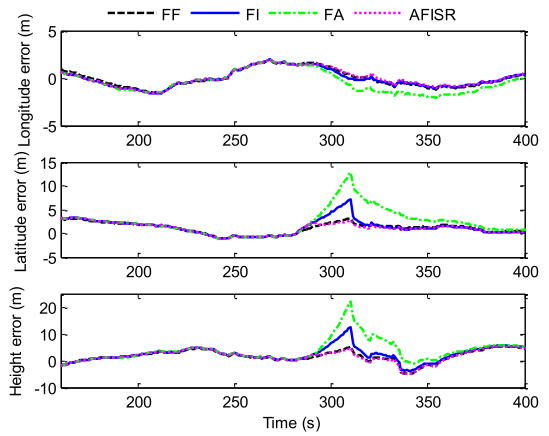

FIGURE 19. The position errors for fault on G11 under the condition of five visible satellites.

TABLE 4. Comparison of the RMS of position errors during fault period.

	RMSE/m	Method			
		FF	FI	FA	AFISR
Geometry 1 (281s~310s)	Longitude	1.23	1.11	1.01	1.23
	Latitude	1.92	4.05	6.59	1.96
	Height	2.68	6.29	10.16	2.82
Geometry 2 (181s~210s)	Longitude	1.06	1.19	1.23	1.19
	Latitude	2.02	2.10	2.13	2.10
	Height	1.94	1.98	1.92	1.98

are shown in Table 4. From Fig. 19 and Table 4, it can be seen that the position errors of these methods in geometry 2 are nearly the same due to the little effect of G11's measurements on the filtering precision, while the difference of position errors between these methods in geometry 1 is very evident. As the measurements of G11 have a great influence on the filtering precision, the position errors of FI increases fast with time. Compared with FI, the position errors of FA are nearly the same as those of FI in the first few seconds, however, when the error accumulates to a certain degree, the position

errors of FA increases faster than FI. Therefore, the FA has the worse filtering precision. The AFISR switches to the new measurement update mode that uses the predicted pseudo-GNSS measurement at 292s, so it has high precision.

VI. CONCLUSION

In this paper, the fault isolation and system reconfiguration for GNSS/INS integration is investigated. The principle and performance of the conventional fault isolation method and fault adaptation method are analyzed and compared in theory. To overcome the drawbacks of them in complex environment, an adaptive fault isolation and system reconfiguration method is proposed. The RBFNN is adopted to predict the pseudo-GNSS measurement when fault is detected, which can be used to conduct the measurement reconfiguration. Besides, an adjustment criterion is introduced to realize the adaptive switch of fault isolation and measurement reconfiguration, which can improve the adaptability to the environment. The theoretical analysis for the comparison of the two traditional methods and the performance of the proposed method are verified by several tests. The main conclusions are listed below.

1) When the measurement of faulty satellite has little effect on the filtering precision, the filtering results of fault isolation and fault adaptation are nearly the same. However, when the measurement of faulty satellite has a great effect on the filtering precision, the fault isolation method can obtain the higher filtering precision than fault adaptation method, especially when the number of visible satellites is small.

2) The proposed predictor based on RBFNN introduces the measurements of INS to provide the motion constraint information. Therefore, compared with the conventional prediction model, it depends less on the motion state of the vehicle and has higher prediction precision.

3) The proposed method can adaptively adjust the fault isolation and system reconfiguration scheme, compared with the traditional methods, it has the better adaptability to the environment, and can improve the precision and reliability of the integration effectively.

In addition, the thresholds of POP and RDPOP have a great influence on the performance of the proposed method, the selection of appropriate values is a key issue and need to be further researched in the future work.

REFERENCES

[1] Y. Liu, X. Fan, C. Lv, J. Wu, L. Li, and D. Ding, "An innovative information fusion method with adaptive Kalman filter for integrated INS/GPS navigation of autonomous vehicles," *Mech. Syst. Signal Process.*, vol. 100, pp. 605–616, Feb. 2018.

[2] M. Alqurashi and J. Wang, "Performance analysis of fault detection and identification for multiple faults in GNSS and GNSS/INS integration," *J. Appl. Geod.*, vol. 9, no. 1, pp. 35–48, Jan. 2015.

[3] T. S. Bruggemann, D. G. Greer, and R. A. Walker, "GPS fault detection with IMU and aircraft dynamics," *IEEE Trans. Aerosp. Electron. Syst.*, vol. 47, no. 1, pp. 305–316, Jan. 2011.

[4] B. Brumback and M. Srinath, "A Chi-square test for fault-detection in Kalman filters," *IEEE Trans. Autom. Control.*, vol. 32, no. 6, pp. 552–554, Jun. 1987.

[5] M. Joerger and B. Pervan, "Kalman filter-based integrity monitoring against sensor faults," *J. Guid., Control, Dyn.*, vol. 36, no. 2, pp. 349–361, Mar. 2013.

[6] L. Wang, K. Zhi, B. Li, and Y. Zhang, "Dynamically adjusting filter gain method for suppressing GNSS observation outliers in integrated navigation," *J. Navigat.*, vol. 71, no. 6, pp. 1396–1412, Nov. 2018.

[7] M. Brenner, "Integrated GPS inertial fault detection availability," in *Proc. Inst. Navigat. 8th Int. Tech. Meeting*, Palm Springs, CA, USA, Sep. 1995, pp. 1949–1958.

[8] C. Call, M. Ibis, J. Mcdonald, and K. Vanderwerf, "Performance of honeywell's inertial/GPS hybrid (HIGH) for RNP operations," in *Proc. IEEE/ION Position, Location, Navigat. Symp.* San Diego, CA, USA: IEEE/ION PLANS, Jan. 2006, p. 244.

[9] Y. C. Lee and D. G. O'Laughlin, "A performance analysis of a tightly coupled GPS/inertial system for two integrity monitoring methods," *J. Navigat.*, vol. 47, no. 3, pp. 175–189, Sep. 2000.

[10] U. I. Bhatti, W. Y. Ochieng, and S. Feng, "Integrity of an integrated GPS/INS system in the presence of slowly growing errors. Part II: Analysis," *GPS Solutions*, vol. 11, no. 3, pp. 183–192, Jan. 2007.

[11] L. Zhong, J. Liu, R. Li, and R. Wang, "Approach for detecting soft faults in GPS/INS integrated navigation based on LS-SVM and AIME," *J. Navigat.*, vol. 70, no. 3, pp. 561–579, May 2017.

[12] U. I. Bhatti, W. Y. Ochieng, and S. Feng, "Performance of rate detector algorithms for an integrated GPS/INS system in the presence of slowly growing error," *GPS Solutions*, vol. 16, no. 3, pp. 293–301, Jul. 2012.

[13] L. Yi-Ting, X. Xiao-Su, L. Xi-Xiang, Z. Tao, L. Yao, Y. Yi-Qing, W. Liang, and T. Jin-Wu, "A fast gradual fault detection method for underwater integrated navigation systems," *J. Navigat.*, vol. 69, no. 1, pp. 93–112, Jan. 2016.

[14] R. Sun, Q. Cheng, G. Wang, and W. Ochieng, "A novel online data-driven algorithm for detecting UAV navigation sensor faults," *Sensors*, vol. 17, no. 10, p. 2243, Sep. 2017.

[15] Y. Zhu, X. Cheng, and L. Wang, "A novel fault detection method for an integrated navigation system using Gaussian process regression," *J. Navigat.*, vol. 69, no. 4, pp. 905–919, Jul. 2016.

[16] Y. Yao, X. Xu, C. Zhu, and C.-Y. Chan, "A hybrid fusion algorithm for GPS/INS integration during GPS outages," *Measurement*, vol. 103, pp. 42–51, Jun. 2017.

[17] S. Hewitson and J. Wang, "Extended receiver autonomous integrity monitoring (eRAIM) for GNSS/INS integration," *J. Surv. Eng.*, vol. 136, no. 1, pp. 13–22, Feb. 2010.

[18] L. Yang, N. L. Knight, Y. Li, and C. Rizos, "Optimal fault detection and exclusion applied in GNSS positioning," *J. Navigat.*, vol. 66, no. 5, pp. 683–700, Sep. 2013.

[19] C. Zhang, X. Zhao, C. Pang, L. Zhang, and B. Feng, "The influence of satellite configuration and fault duration time on the performance of fault detection in GNSS/INS integration," *Sensors*, vol. 19, no. 9, p. 2147, May 2019.

[20] P. J. G. Teunissen, "An integrity and quality control procedure for use in multi sensor integration," in *Proc. 3rd Int. Tech. Meeting Satell. Division Inst. Navigat.*, Colorado Springs, CO, USA, Sep. 1990, pp. 513–522.

[21] P. J. G. Teunissen, "Distributional theory for the DIA method," *J. Geodesy*, vol. 92, no. 1, pp. 59–80, Jan. 2018.

[22] W. Jiang, Y. Li, and C. Rizos, "A multisensor navigation system based on an adaptive fault-tolerant GOF algorithm," *IEEE Trans. Intell. Transp. Syst.*, vol. 18, no. 1, pp. 103–113, Jan. 2017.

[23] M. A. Gandhi and L. Mili, "Robust Kalman filter based on a generalized maximum-likelihood-type estimator," *IEEE Trans. Signal Process.*, vol. 58, no. 5, pp. 2509–2520, May 2010.

[24] C. Yang, A. Mohammadi, and Q.-W. Chen, "Multi-sensor fusion with interaction multiple model and chi-square test tolerant filter," *Sensors*, vol. 16, no. 11, p. 1835, Nov. 2016.

[25] C. Jiang, S.-B. Zhang, and Q.-Z. Zhang, "A new adaptive h-infinity filtering algorithm for the GPS/INS integrated navigation," *Sensors*, vol. 16, no. 12, p. 2127, Dec. 2016.

[26] Y. Yang and W. Gao, "Comparison of adaptive factors in Kalman filters on navigation results," *J. Navigat.*, vol. 58, no. 3, pp. 471–478, Sep. 2005.

[27] G. Hu, S. Gao, and Y. Zhong, "A derivative UKF for tightly coupled INS/GPS integrated navigation," *ISA Trans.*, vol. 56, pp. 135–144, May 2015.

[28] S. Zaminpardaz and P. J. G. Teunissen, "DIA-datasnooping and identifiability," *J. Geodesy*, vol. 93, no. 1, pp. 85–101, Jan. 2019.

[29] Q. Xu, X. Li, and C.-Y. Chan, "Enhancing localization accuracy of MEMS-INS/GPS/in-vehicle sensors integration during GPS outages," *IEEE Trans. Instrum. Meas.*, vol. 67, no. 8, pp. 1966–1978, Aug. 2018.
[30] X. Tan, J. Wang, S. Jin, and X. Meng, "GA-SVR and pseudo-position-aided GPS/INS integration during GPS outage," *J. Navigat.*, vol. 68, no. 4, pp. 678–696, Jul. 2015.
[31] S. Adusumilli, D. Bhatt, H. Wang, V. Devabhaktuni, and P. Bhattacharya, "A novel hybrid approach utilizing principal component regression and random forest regression to bridge the period of GPS outages," *Neurocomputing*, vol. 166, pp. 185–192, Oct. 2015.
[32] X. Lei and J. Li, "An adaptive navigation method for a small unmanned aerial rotorcraft under complex environment," *Measurement*, vol. 46, no. 10, pp. 4166–4171, Dec. 2013.
[33] X. Chen, C. Shen, W.-B. Zhang, M. Tomizuka, Y. Xu, and K. Chiu, "Novel hybrid of strong tracking Kalman filter and wavelet neural network for GPS/INS during GPS outages," *Measurement*, vol. 46, no. 10, pp. 3847–3854, Dec. 2013.
[34] L. Chen and J. Fang, "A hybrid prediction method for bridging GPS outages in high-precision POS application," *IEEE Trans. Instrum. Meas.*, vol. 63, no. 6, pp. 1656–1665, Jun. 2014.
[35] Z. Wu and W. Wang, "INS/magnetometer integrated positioning based on neural network for bridging long-time GPS outages," *GPS Solutions*, vol. 23, p. 88, Jul. 2019, doi: 10.1007/s10291-019-0877-4.
[36] C.-P. Pang and Z.-Z. Liu, "Bridging GPS outages of tightly coupled GPS/SINS based on the adaptive track fusion using RBF neural network," in *Proc. IEEE Int. Symp. Ind. Electron.* Seoul, South Korea: Seoul Olympic Parktel, Jul. 2009, pp. 960–965.

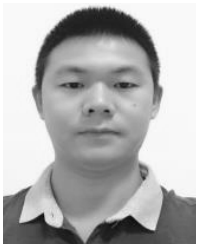

CHUANG ZHANG received the B.Sc. degree in navigation engineering and the M.Sc. degrees in communication and information system from the Information and Navigation College, Air Force Engineering University, Xi'an, China, in 2014 and 2016, respectively, where he is currently pursuing the Ph.D. degree with the Information and Navigation College.

His research interests include GNSS/INS integrated filtering algorithm, and fault detection and isolation method.

XIUBIN ZHAO was born in China, in 1965. He received the B.Sc. degree from the Telecommunication Engineering Institute, Air Force Engineering University, Xi'an, China, in 1988, the M.Sc. degree in astronautics from the School of Electronic Information, Nanjing University of Aeronautics, Nanjing, China, in 1991, and the Ph.D. degree from the School of Electronic and Information, Northwestern Polytechnical University, Xi'an, in 2006.

He is currently a Full Professor with the Information and Navigation College, Air Force Engineering University. His research interests include GNSS and its integrated navigation systems, and aircraft navigation and control.

CHUNLEI PANG received the B.Sc. degree in navigation engineering and the M.Sc. degrees in communication and information system from the Telecommunication Engineering Institute, Air Force Engineering University, Xi'an, China, in 2007 and 2009, respectively, and the Ph.D. degree from the Information and Navigation College, Air Force Engineering University, Xi'an, in 2013.

He is currently a Lecturer with the Information and Navigation College, Air Force Engineering University. His research interests include GNSS high-precision positioning and GNSS/INS integrated navigation.

TENGYAO LI received the B.Sc. and M.Sc. degrees in computer science from the Information and Navigation College, Air Force Engineering University, Xi'an, China, in 2014 and 2016, respectively, where he is currently pursuing the Ph.D. degree with the Information and Navigation College.

His research interest includes attack detection and resilient recovery on ADS-B Data.

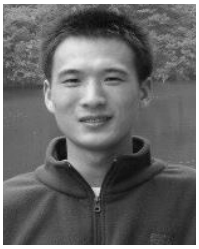

LIANG ZHANG received the B.Sc. degree in surveying engineering from the School of Geodesy and Geomatics, Wuhan University, Wuhan, China, in 2010, and the Ph.D. degree in aeronautical and astronautical science and technology from the College of Aerospace and Engineering, National University of Defense Technology, Changsha, China, in 2013.

He is currently a Lecturer with the Information and Navigation College, Air Force Engineering University. His research interest includes GNSS/SINS integrated navigation and its high-precision data processing.